

Study of the formation and anti-corrosion properties of Zn—Al hydrotalcite conversion films grown “in situ” on different zinc alloys coated steel

Thu Thuy Pham^{a,b}, Thuy Duong Nguyen^a, Anh Son Nguyen^a, Maurice Gonon^b, Xavier Noirfalise^c, Yoann Paint^c, Thi Xuan Hang To^{a,d}, Marie-Georges Olivier^{b,c,*}

^a Institute for Tropical Technology, Vietnam Academy of Science and Technology, 18 Hoang Quoc Viet, Cau Giay, Hanoi, Viet Nam

^b Université de Mons, Materials Science Department, Place du Parc 20, Mons, Belgium

^c Materia Nova, Parc Initialis, Mons, Belgium

^d Graduate University of Science and Technology, Vietnam Academy of Science and Technology, 18 Hoang Quoc Viet, Cau Giay, Hanoi, Viet Nam

ARTICLE INFO

Keywords:

Zn—Al hydrotalcite conversion films

Zinc alloys coated steel

Anti-corrosion

ABSTRACT

The Zn-Al-CO₃²⁻ hydrotalcite (HT) conversion film was developed on hot-dip galvanized steel (HDG), Zn—Al coated steel (ZA), and Zn-Al-Mg coated steel (ZAM) substrates by “in situ” growth process for Al³⁺/Zn²⁺ ratio of 5/3 at pH 12. The characteristics of all the Zn—Al HT film-coated samples before and after exposure to 0.1 M NaCl for 24 h were investigated by means of Fourier-transform infrared (FT-IR), X-Ray Diffraction (XRD), electron microscopy/energy dispersive X-ray spectroscopy SEM/EDS, and X-ray photoelectron spectroscopy (XPS). The corrosion properties of all the samples were studied by open circuit potential measurements (OCP), polarization curves, and electrochemical impedance spectroscopy (EIS). The electrochemical tests indicated that the HT film-coated can significantly restrain the corrosion of the HDG, ZA, and ZAM substrates but this efficiency was depending on the alloying compounds of the sacrificial layer. The inhibitive effect of HT film-coated on all the corrosion substrates was discussed in detail.

1. Introduction

The zinc coatings can provide both a barrier and sacrificial protection to the steel and its alloy surface, thus it has been widely applied for the corrosion protection of the steel alloys [1]. In order to enhance the corrosion protection of zinc coatings without rising coating thickness, the addition of aluminum and/or magnesium to the coating systems is a promising approach [2]. The corrosion potentials of Al and Mg were more negative than that of Zn, thus the addition of Al and/or Mg to zinc coating can provide more sacrificial protection than that of pure one [3]. Moreover, the enhanced corrosion protection of zinc alloys as Zn—Al, Zn—Mg, and Zn-Al-Mg coatings has been also attributed to the density of new corrosion products after immersion in aggressive environments, which can impede oxygen diffusion [4,5].

Due to their unique lamellar structure, hydrotalcites (HT) can trap and hold aggressive corrosive anions as chloride in their positively charged layers [6]. Moreover, hydrotalcites can also encapsulate and release corrosion inhibitors, which provide them additional advantages for corrosion protection [6,7]. Recently, hydrotalcites intercalated with

inorganic or organic compounds were widely investigated as layered anti-corrosion materials when incorporated into organic coatings [6–9] and sol-gel coatings [10–12]. They significantly improve the coating's barrier properties and corrosion inhibition of the metal/coating surfaces due to their different functional groups [7]. Nguyen et al. prepared and compared the anti-corrosion performance of Zn—Al HT modified with benzoate (BZ), 2-benzothiazolythio-succinic acid (BTSA), and sebacate (SB) on carbon steel [6,7]. HT-SB showed higher inhibiting efficiency than those of HT-BZ and HT-BTSA. Moreover, 1.5 wt% HT-SB, HT-BZ, and HT-BTSA were used as inhibitor nanocontainers in epoxy coatings applied on carbon steel. They were easily dispersed and enhanced the barrier properties of the organic coating [7]. MgAl HT was used as inhibitor nanocontainers (1.5 and 10 %, w/w) to be incorporated into sol-gel coatings on AA2024-T3 alloy substrate [11]. The corrosion protection of the AA2024-T3 alloy substrate was enhanced significantly at higher weight percentages of HT added to the hybrid sol-gel coating.

Moreover, hydrotalcites can be directly developed on the metal surface and form physical protective films avoiding the exposure of the substrate to aggressive environments [13,14]. Zn—Al HT films [15],

* Corresponding author at: Université de Mons, Materials Science Department, Place du Parc 20, Mons, Belgium.

E-mail address: marjorie.olivier@umons.ac.be (M.-G. Olivier).

<https://doi.org/10.1016/j.porgcoat.2022.107221>

Received 31 May 2022; Received in revised form 9 August 2022; Accepted 21 September 2022

Available online 29 September 2022

0300-9440/© 2022 Elsevier B.V. All rights reserved.

Ni—Al HT films [16], Mg—Al HT films [14], and Ca—Al HT films [17] were fabricated on aluminum alloys by using in-situ hydrothermal treatment method. The results presented that these hydrotalcite films showed high flexibility in terms of control of the structure and morphology of the films with the expected micro/nanostructure and controlled crystal orientation. The corrosion resistance of the aluminum substrate treated with HT films was highly improved [14,17]. Mg—Al HT films [18,19] and Zn—Al HT films [20], which consisted of uniform hexagonal nanoplates, were prepared through the combination of the co-precipitation and hydrothermal methods on the AZ31 magnesium alloy. It was found that these Mg—Al HT and Zn—Al HT can act as smart coatings responding to stimuli and giving self-healing ability in the corrosive environment. Mg—Al HT films modified with 8-quinolinol showed significant improvement in anti-corrosion properties and provided excellent protection after immersion in NaCl solution for one month [21].

The preparation of HT modified with different inorganic and organic inhibitors was mainly investigated on substrates such as Mg and Al alloys, however, the growth of HT films on zinc alloys and galvanized steel has rarely been reported. Mikhailau et al. prepared nitrate anions intercalated Zn—Al HT film on zinc alloy by dipping the substrates into a $\text{Al}(\text{NO}_3)_3$ solution containing NaNO_3 at pH 3.2 [22,23]. The Zn—Al— CO_3^{2-} HT were developed on galvanized steel substrates by immersing bare substrates in high alkaline sodium aluminate solutions at different pH values [24–26]. They found that ZnOH^+ and $\text{Al}(\text{OH})_4^-$ were the two main species for HT layers formation on zinc substrates in acid solutions [22], while $\text{Zn}(\text{OH})_5^-$ and $\text{Al}(\text{OH})_4^-$ species were considered as the HT building blocks on galvanized steel in alkaline solutions [26]. In our previous research, we proved that the Al/Zn ratio influenced the morphology, thickness, and anti-corrosion of Zn—Al HT films on a pure zinc sacrificial layer obtained by electrodeposition process (EG) [27]. In addition, the excellent anti-corrosion functionalities of these HT films attributed to their physical barrier function, ion-exchange, and protective deposition of ZnO were demonstrated on this pure zinc layer.

Uan et al. [28–30] and Chen et al. [31,32] prepared the Mg—Al HT films on Mg alloys containing different aluminum contents in the substrate by immersing the bare substrates in a carbonic acid solution. They found that the composition of Mg alloys affected the “in situ” growth of HT films, their morphology, as well as their corrosion protection. However, from the best of our knowledge, the “in situ” growth of Zn—Al HT films has not been extended to zinc alloys as Zn—Al, Zn—Al—Mg, and Zn—Mg alloys coated steel substrates. In addition, the role of Mg and Al alloying elements on the “in situ” growth of HT films has not been further studied and discussed. Our previous results obtained on EG steel substrate [27] motivated us to continue studies on formation and anti-corrosion of Zn—Al HT film developed directly on different zinc alloys coated steel substrates. Moreover, the effect of Al and Mg contents from substrate's top layer on formation mechanism, structure, and properties of HT films on these substrates was investigated and explained. The Zn—Al HT conversion films were synthesized using Al/Zn ratio of 5/3 at pH 12 on different zinc alloys coated steel substrates. The structure and surface morphology of these Zn—Al HT films were observed by FT-IR, XRD, XPS, and SEM/EDS. The anti-corrosion performance of these HT films was determined by using electrochemical methods. By analyzing the characterization of corrosion products and interpreting the electrochemical results, the inhibitive effect of HT films on corrosion zinc alloys coated steel was highlighted and discussed depending on their Mg and Al contents.

2. Experimental method

2.1. Materials

The hot-dip galvanized steel (HDG), Zn—Al coated steel (ZA), and Zn—Al—Mg coated steel (ZAM) substrates were prepared and supplied by Arcelor Mittal (Belgium). The cross-sectional microstructure and

chemical compositions of these substrates were observed under Hitachi SU8020 FE-SEM. The element compositions and the thickness of the top layer of these substrates are given in Table 1. The roughness of top layers was determined by optical profilometry with the NanoJura instrument as described in our previous publication [27]. The R_a values of bare substrates were also presented in Table 1. The specimens were cut to 25×50 mm. Prior to the synthesis experiment, the substrates were ultrasonically cleaned in acetone for 25 min, rinsed with DI water, further, cleaned using a commercial alkaline solution Gardoclean (10 g/l) for 30 s, finally, washed with DI water, ethanol (EtOH), and dried in cool air.

EtOH and NaCl were provided by VWR. $\text{Al}(\text{NO}_3)_3 \cdot 9\text{H}_2\text{O}$ from Sigma Aldrich, $\text{Zn}(\text{NO}_3)_2 \cdot 7\text{H}_2\text{O}$ from Fluka, and NaOH from VWR were used to synthesize the Zn—Al HT films on zinc alloys coated steel.

2.2. Experimental details

In this research, the Zn—Al HT film synthesis procedure was performed as described in our previous publication [27]. The Zn—Al HT films on HDG, ZA, and ZAM substrates, which were named as HT-HDG, HT-ZA, and HT-ZAM respectively were synthesized by the “in situ” growth process. The HT films were grown in a reactional bath containing 0.05 M $\text{Al}(\text{NO}_3)_3$ and 0.03 M $\text{Zn}(\text{NO}_3)_2$ (pH adjusted to 12 using 1 M NaOH) at room temperature for 6 h with stirring and maintained hereafter in the solution for 16 h without stirring. The as-prepared HT film samples were washed with DI water, EtOH, and finally dried at 70°C for 2 h.

The cross-section of all the bare substrates and Zn—Al HT samples was also analyzed as described in our previous paper [27] after embedding by an epoxy resin (provided by Stuers), and then polishing from 400 to 4000 by SiC papers.

2.3. Methods and analyses

2.3.1. Characterization

Fourier-transform infrared (FT-IR) of the obtained Zn—Al HT films were recorded on Bruker IFS 66 v/S between 500 and 4000 cm^{-1} in ATR working mode.

The X-Ray Diffraction (XRD, Bruker D5000) with $\text{CoK}\alpha$ (wavelength = 0.1789 nm) and Fe filter over the 2θ range from 10° to 70° at rate of 1° min^{-1} was used to observe the crystalline structure of all the substrates uncovered and covered with Zn—Al HT films before and after exposure to 0.1 M NaCl.

The chemical compositions, surface morphology, and thickness of the bare substrates and Zn—Al HT coated samples before and after immersion in 0.1 M NaCl were analyzed using FE-SEM (Hitachi SU8020) with an energy dispersive X-ray spectroscopy (EDX, Thermo Scientific Noran System 7).

The extreme surface characterization of Zn—Al HT films was investigated by X-ray photoelectron spectroscopy (XPS) using an ESCA-5000 (Physical Electronics) Versa Probe system with a monochromatic Al $\text{K}\alpha$ radiation at 1486.6 eV . The XPS measurements were recorded by an X-Ray source with beam size diameter of $200\text{ }\mu\text{m}$ and the power was 50 W . Atomic compositions were derived from peak areas after a Shirley

Table 1
Element compositions, thickness, and roughness of top layer on the different zinc alloys coated steel substrates.

Substrates	Element content (wt%)					Thickness (μm)	R_a (μm)
	Zn	Al	C	O	Mg		
HDG	92.1	1.2	3.9	2.8	–	11.6 ± 0.2	0.871 ± 0.015
ZA	82.9	9.4	3.0	4.7	–	17.5 ± 0.1	1.225 ± 0.052
ZAM	83.6	7.2	2.4	2.8	4.0	29.0 ± 0.1	0.012 ± 0.002

background subtraction.

2.3.2. Electrochemical measurements

The electrochemical inspection of the bare substrates with and without Zn–Al HT films was investigated by electrochemical measurements as open circuit potential (OCP), electrochemical impedance spectroscopy (EIS), and potentiodynamic polarizations (Parstat Model 2273 controlled by Powersuite® software), using a conventional three-electrode system in which a large platinum electrode, substrates with an exposed area of 1 cm², and an Ag/AgCl (sat. KCl) were the auxiliary, working and reference electrodes, respectively. The stability of the OCP was previously checked for 24 h in 0.1 M NaCl. The EIS measurements were also determined in 0.1 M NaCl solution by using a peak-to-peak sinusoidal voltage amplitude of 5 mV in the frequency domain of 10⁵ Hz to 10⁻² Hz with 50 points. The potentiodynamic polarization curves were recorded after 24 h of exposure to 0.1 M NaCl from -30 mV to 400 mV vs OCP (V / Ag/AgCl) at 0.2 mV s⁻¹.

3. Results and discussion

3.1. Characterization and surface morphology of the Zn–Al HT conversion films on different zinc alloys coated steel substrates

All the studied substrates were zinc alloys coated steel with different contents of Al and Mg (Table 1). The Al content of the HDG, ZA, and ZAM substrates was 1.2, 9.4, and 7.2 wt%, respectively. The presence of Mg in ZAM substrate was 4.0 wt%. The thickness of ZAM layer was 29.0 μm considerably higher than those of ZA (17.5 μm) and HDG (11.6 μm) coatings (Fig. 1). In contrast, the R_a value of ZAM substrate was 0.012 μm, which was significantly lower than those of other substrates (Table 1). The previous research indicated that the morphology and composition of the substrate had obvious affection to the “in situ” development mechanism, structure, and morphology of HT films [31,32], thus this chapter will discuss the growth of Zn–Al-HT films on different zinc alloys.

The FT-IR spectra of Zn–Al HT films on zinc alloys substrates were measured and presented in Fig. 2. All the HT films presented an absorption band at about 3420 cm⁻¹, which corresponds to the stretching vibration of crystal water and hydroxyl groups in the brucitelike layers [21]. In addition, the peak around 1600 cm⁻¹ was ascribed to the bending vibration of H₂O molecules which was attributed to interlayer H₂O molecules of HT films, and these absorbed ones on the HTs surface [33]. The strong bands at 1350 cm⁻¹ originated from the characteristic band of symmetric and asymmetric stretching vibrations of CO₃²⁻ from taken up by CO₂ in the air [26,27]. Moreover, the lower wavenumber bands 500–800 cm⁻¹ were attributed to the lattice vibration of the metal (e.g. M–O, M–O–M, O–M–O) [33].

XRD patterns of HDG, ZA, and ZAM substrates uncovered and covered with the Zn–Al HT films were displayed in Fig. 3a, b, and c, respectively. The diffraction peaks at 2θ values of 42.50°, 45.70°, 50.80°, and 64.00°, corresponding to the (101), (102), (103), and (110) lattice planes (JCPDS No. 00–004-0831) of zinc, were observed for all

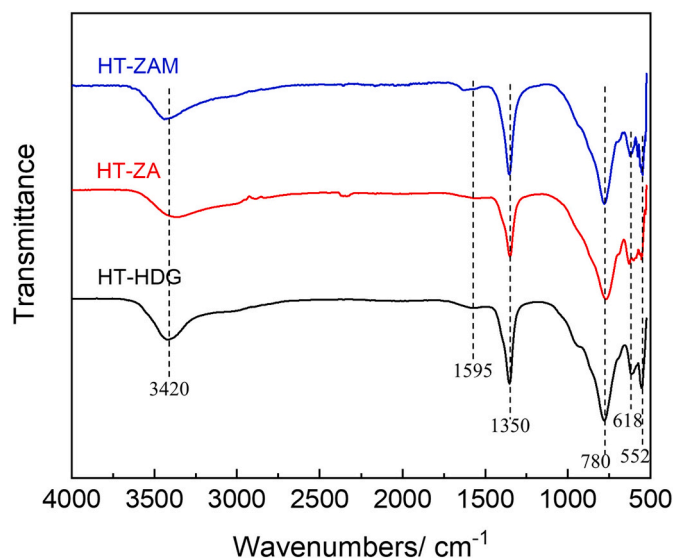


Fig. 2. The FT-IR spectrum of the Zn–Al HT films on the HDG, ZA and ZAM substrates.

bare substrates and the HT films. Iron (JCPDS No. 00–006-0696) and aluminum (JCPDS No. 00–004-0787) were present for all the samples. Moreover, the strong peaks of magnesium zinc – MgZn₂ (JCPDS No. 00–034-0457) were easily observed in the XRD pattern of ZAM and HT-ZAM. Compared with all bare substrates, the new peaks at about 13.50°, 27.40°, and 40.50°, which correspond respectively to the characteristic (003), (006), and (012) diffraction peaks of Zn₆Al₁₂(OH)₁₆(CO₃²⁻)·4H₂O HT (JCPDS No. 00–038-0486), indicated that Zn–Al HT intercalated with carbonate anions films were successfully developed on HDG, ZA, and ZAM substrates by using the “in-situ” method.

The lattice parameters, corresponding to the cation–cation distance within the brucite layer (a) and the thickness of the interlayer distance (c), were estimated by $a = 2 \times d_{(110)}$ and $c = 3 \times d_{(003)}$, respectively (Table 2) [34,35]. The crystallite size (d) of HTs was calculated by using the Scherrer equation at the strongest characteristic peak (003) [27]:

$$d = \frac{0.9 \times \lambda}{\text{FWHM} \times \cos\theta}$$

where $\lambda = 0.1789$ nm (the wavelength of X-rays (Co K0α₁)), FWHM: the full width at half maximum in radians, and θ : the diffraction angle for (003). The a and c values of the Zn–Al HT were not significantly different on all substrates and were quite similar to HT films for Al/Zn ratio of 5/3 on EG steel (HT 5/3) [27]. The crystallite size (d) of HT-HDG was not much different from that of HT 5/3 sample [27], however, it was much larger than those of HT-ZA and HT-ZAM. The increase of Al and Mg concentration in the metallic layer composition affected the HT deposition process, thus the HT-ZA and HT-ZAM crystallite size showed a significant difference from that of HT-HDG.

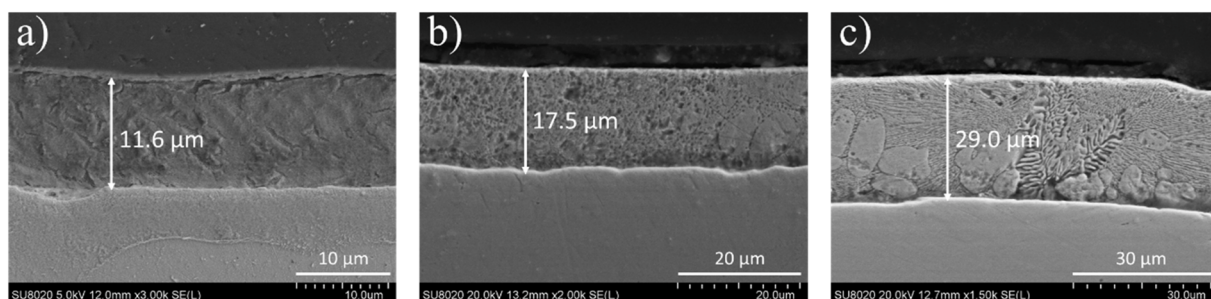


Fig. 1. SEM of the cross-sections of HDG (a), ZA (b), and ZAM (c) substrates.

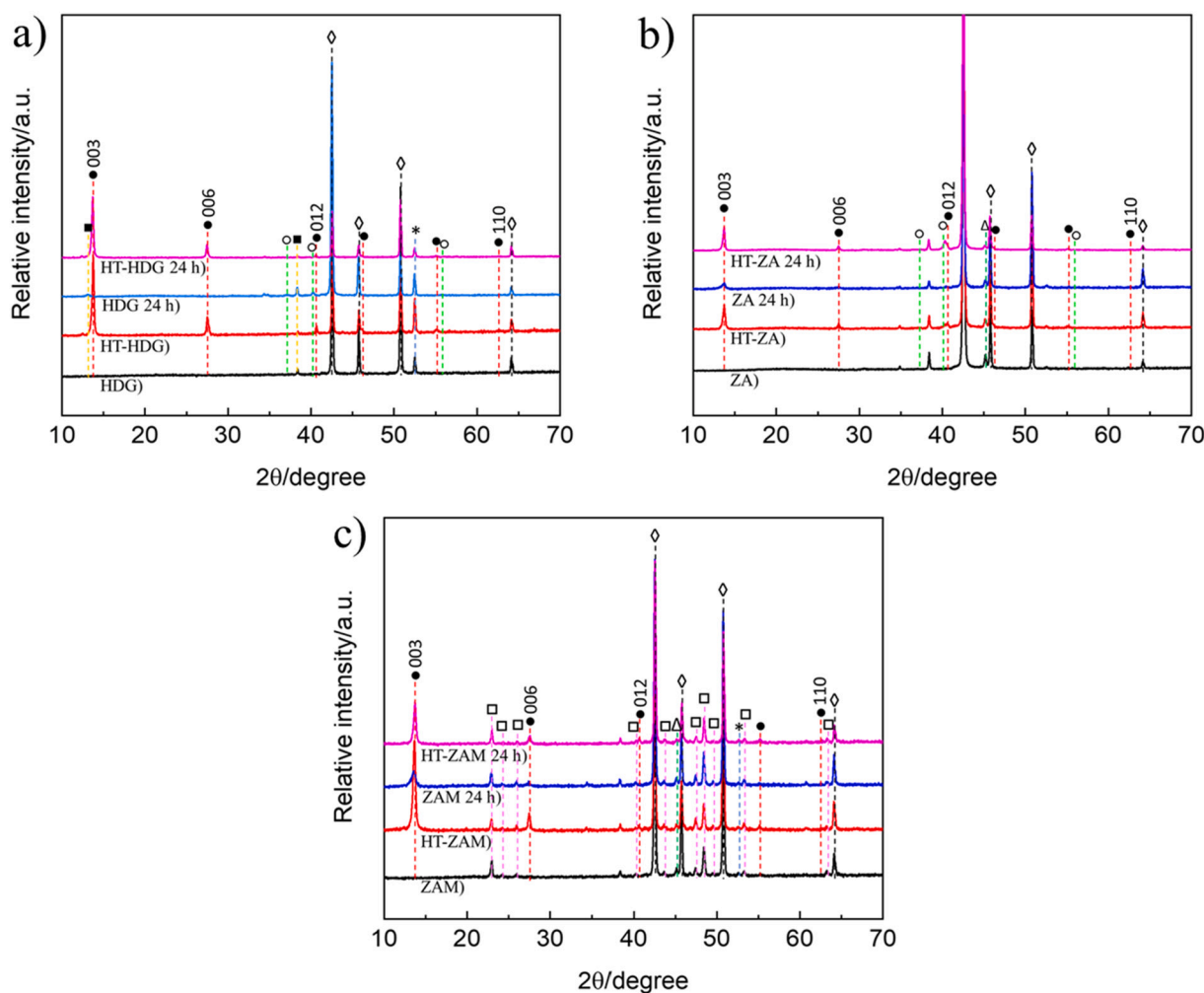


Fig. 3. XRD patterns of the HDG and HT-HDG samples (a), ZA and HT-ZA samples (b), and, ZAM and HT-ZAM samples (c) before and after exposure to 0.1 M NaCl for 24 h. Peaks marked with ●, ◇, △, □, *, ○, and ■ are contributed to Zn—Al HT, Zn, Al, MgZn₂, Fe, ZnO, and Zn₅(OH)₈Cl₂·H₂O/ZnCl₂·4Zn(OH)₂·H₂O, respectively.

Table 2

The indexing of XRD for the Zn—Al HT film on the HDG, ZA, and ZAM substrates before and after exposure to 0.1 M NaCl for 24 h.

Parameter (nm)	HT-HDG	HT-ZA	HT-ZAM	HT-HDG 24 h	HT-ZA 24 h	HT-ZAM 24 h
d(003)	0.752	0.758	0.759	0.759	0.764	0.765
d(006)	0.377	0.379	0.378	0.379	0.381	0.381
d(110)	0.172	0.173	0.173	0.172	0.173	0.173
Lattice parameter a	0.344	0.346	0.346	0.344	0.346	0.346
Lattice parameter c	2.256	2.274	2.277	2.277	2.293	2.295
Crystallite size d	38.6	29.7	28.9	35.6	27.3	26.8
(003)/(006) peak height ratio	4.2	4.0	4.7	3.5	3.2	3.4

The morphology of HT films grown on the HDG, ZA, ZAM substrates was presented in Fig. 4. The surface of HT film on all the substrates highlighted the rough hillocky structures, which was observed from the SEM images at lower magnifications, indicating that the deposition of HT crystallites on the substrate surfaces was quite homogeneous. The amount of HT crystallites, which were deposited on the HDG surface, was more than the other two surfaces. It can be easily observed from

Fig. 4.d1, h1, and m1 that the hexagonal crystallites of HT were relatively similar on the different substrate surfaces. Comparing the morphology of the HT crystallites close to the surfaces (Fig. 4.d2, h2, and m2), the differences can be observed. The SEM image of HT-HDG film at high magnification showed a rose petal-like nanostructure of HT crystallites, however, its structure was not sheet-like but cluster-like (Fig. 4.d2). In contrast, the SEM image of HT-ZA film at the same magnification indicated that the vertical growth of HT nanoplates became denser and more uniform on this substrate (Fig. 4.h2), which can be expected to increase the efficiency for preventing the penetration of aggressive corrosive anions, thus enhancing the anti-corrosion of the ZA substrate. The HT crystallites with the sheet-like structure were developed vertically on the ZAM substrate (Fig. 4.m2), however, some gaps were observed on the surface, which may negatively affect the corrosion protection of this HT film. The composition of HT films formed on all the substrates were analyzed by EDS (Table 3). The main chemical compositions of all the HT films were Zn, Al, O, and C elements. The compositions of HT films were significantly different in each region. The O and Al contents at the HT-HDG 1 (Fig. 4.d1), HT-ZA 1 (Fig. 4.h1), and HT-ZAM 1 zones (Fig. 4.m1) were significantly higher than those of HT-HDG 2 (Fig. 4.d2), HT-ZA 2 (Fig. 4.h2), and HT-ZAM 2 (Fig. 4.m2) ones, respectively, indicating that the amount of HT crystallites deposited in these regions, was larger.

In addition, the composition and chemical state of the top surface of Zn—Al HT films on HDG, ZA, and ZAM substrates were deeply explored by XPS (Fig. 5). From the survey spectrum of all HT film samples, the

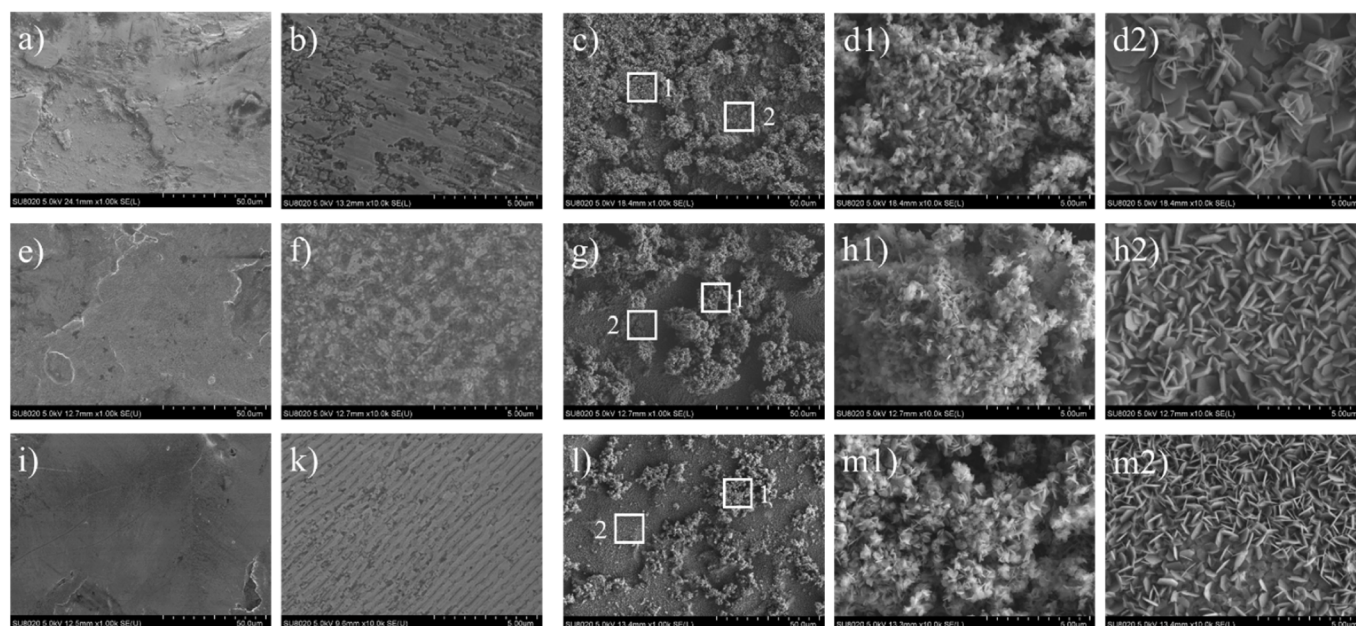


Fig. 4. SEM images of the HDG (a, b), HT-HDG (c, d1, d2), ZA (e, f), HT-ZA (g, h1, h2), ZAM (i, k), and HT-ZAM (l, m1, m2) samples.

Table 3

Element contents obtained from the EDS results of the HT films on the HDG, ZA, and ZAM substrates.

Sample	Element content (wt%)				
	Zn	Al	O	C	Mg
HT-HDG 1	46.8	9.6	40.5	2.1	–
HT-HDG 2	66.7	4.9	20.8	2.0	–
HT-ZA 1	40.9	12.0	45.3	1.8	–
HT-ZA 2	72.2	6.0	20.6	1.2	–
HT-ZAM 1	57.4	7.9	31.9	1.5	1.4
HT-ZAM 2	72.9	4.9	17.9	1.2	3.0

typical spectral peaks, corresponding to Zn, Al, C, and O, were detected. For the HT-ZAM survey spectrum, the typical spectral peaks attributed to Mg were not observed, indicating that magnesium contained in the zinc layer did not participate in the growth process of the HT conversion film. The twin peaks at 1022.0 and 1045.0 eV were ascribed to Zn 2p_{3/2} and Zn 2p_{1/2}, respectively, confirming the presence of the divalent oxidation state of Zn element in Zn–Al HT from the Zn 2p XPS spectrum of all HT samples [36]. The 74.3 eV peak of Al 2p corresponded to the trivalent oxidation state of Al element in Zn–Al HT (Fig. 5. a3, b3, and c3) [36]. The presence of three different carbon-containing functional groups at 289.8, 286.4 and 284.9 eV associated to O–C=O, C–O, and C–C bonds of carboxylate intercalated HT were observed in Fig. 5. a4, b4, and c4, respectively [37].

The cross-section views and EDS maps of the HT films on HDG, ZA, and ZAM substrates embedded in resin were shown in Fig. 6. Similarly with the EDS map of HT 5/3 on the EG steel surface [27], the Zn–Al HT films with the distribution of Zn, Al, O, and C elements were developed on all the substrates. The thickness of HT films on HDG, ZA, and ZAM substrates were about 9.1 ± 0.1 , 14.6 ± 0.1 , and 7.2 ± 0.6 μm , respectively. The amount of crystalline HT deposited on the ZA substrate was larger than those of HDG and ZAM substrates. Moreover, the tightness of the HT-ZA films was better than the other two HT films, which was more favorable to avoid the substrate being exposed to aggressive environments. The higher content in aluminum in the ZA substrate can probably furnish trivalent Al cations during immersion which can participate in the HT growth (Table 3). In the case of the ZAM substrate, the preferential dissolution of magnesium prevents the

aluminum dissolution and inhibits the HT growth formation. The magnesium was not involved in the HT structure as proved by XPS experiments.

3.2. Corrosion products of the Zn–Al HT conversion films on different zinc alloys coated steel substrates after 24 h of exposure to 0.1 M NaCl

The XRD patterns of all the samples after 24 h of exposure to 0.1 M NaCl were presented in Fig. 3. It can be noted that the main corrosion product on the bare HDG substrate was simonkolleite - Zn₅(OH)₈Cl₂·H₂O/ZnCl₂·4Zn(OH)₂·H₂O (JCPDS No. 00–007-0155), while Zn–Al–CO₃ HT was the main corrosion product formed on the bare ZA and ZAM substrates after 24 h immersion. Besides, the characteristic peaks of zincite - ZnO (JCPDS No. 00–036-1451) were also detected in the corrosion products of HDG and ZA substrates [1]. The characteristic peaks of Zn–Al–CO₃ HT crystallites can be easily observed on the XRD patterns of all the HT films after 24 h. However, the intensity of these diffraction peaks showed a slight decrease. Moreover, the peak position of the (003) of all the HT films shifted to a lower angle of approximately 0.1° (Fig. 7), confirming that Cl[–] ions were intercalated due to ion exchange, which is in agreement with our previous research [27]. These results showed that the carbonate-containing HT films on all the zinc coated steel substrates offered high durable properties and acted as effective chloride “nanotraps”, therefore, these HT films can be expected to delay substrate’s surface degradation. Compared with the original HT crystallites, the crystallite size of all HT had a significant decrease after 24 h of immersion, indicating that the HT crystallites were partially dissolved (Table 2). In addition, the low intensity peaks of ZnO were also found on the XRD patterns of the HT-HDG and HT-ZA films after 24 h of immersion, implying the solid phase re-deposition of Zn²⁺ cations from the partial dissolution of the Zn alloys substrates and Zn–Al HT films [27,38]. However, the ZnO characteristic peaks cannot be observed in the XRD pattern of ZAM and HT-ZAM. The buffering effect of Mg dissolution from the ZAM surface resulted in an inhibition of the formation of ZnO, thus the amount of ZnO crystallites was very small and cannot be detected on the ZAM and HT-ZAM surfaces by XRD analysis [4].

The peaks for all chemical elements of the Zn–Al HT films after 24 h of exposure to 0.1 M NaCl were showed in the XPS survey spectra (Fig. 8). Chloride was not detected by XPS after 24 h of immersion,

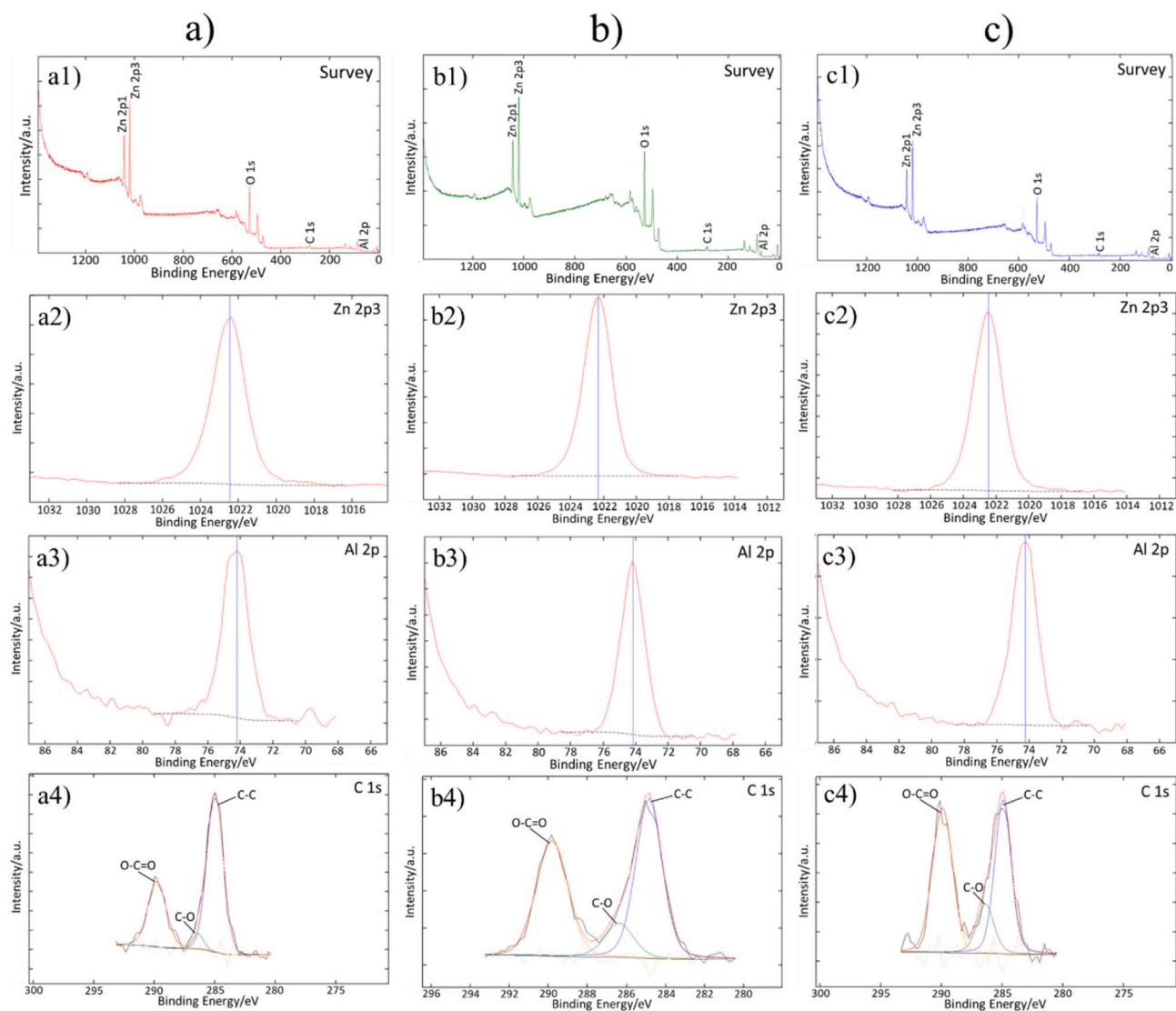


Fig. 5. Survey and high resolution XPS spectra of the HT-HDG (a), HT-ZA (b), and HT-ZAM (c) films.

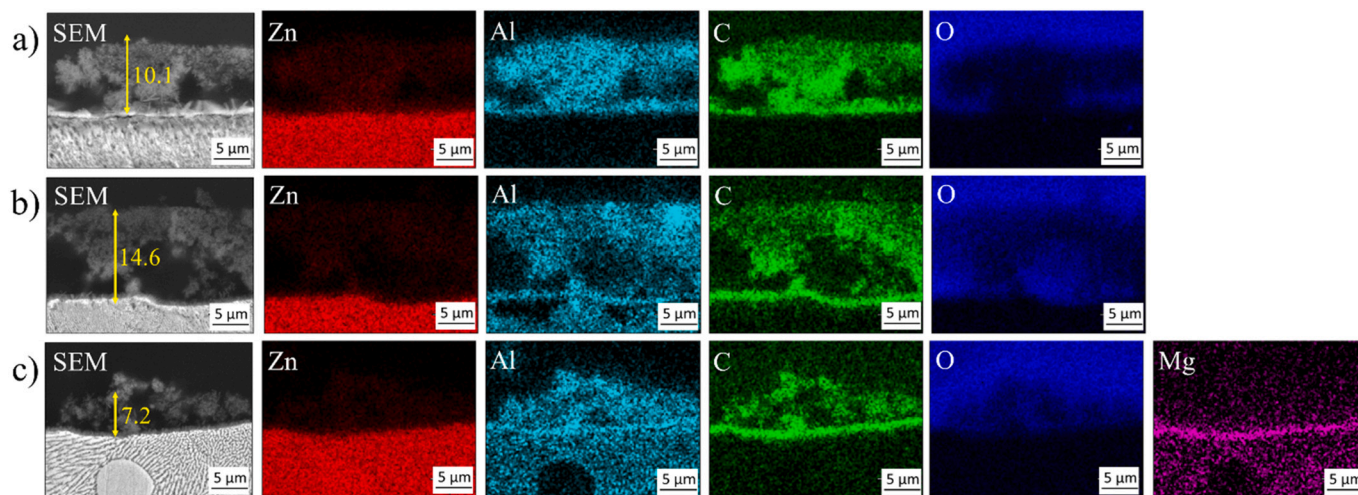


Fig. 6. SEM and EDS maps of the cross-sections of all the HT films on HDG (a), ZA (b), ZAM (c) substrates.

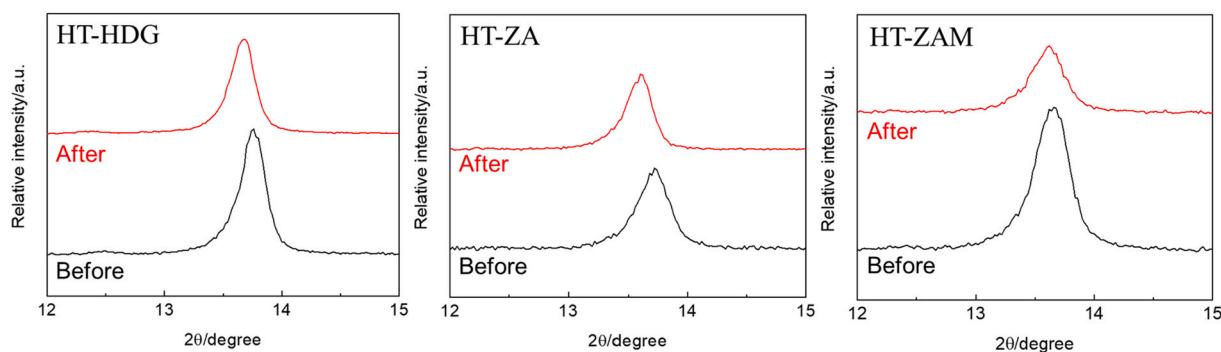


Fig. 7. XRD patterns from 12° to 15° of the HT-HDG, HT-ZA, and HT-ZAM films before and after exposure to 0.1 M NaCl for 24 h.

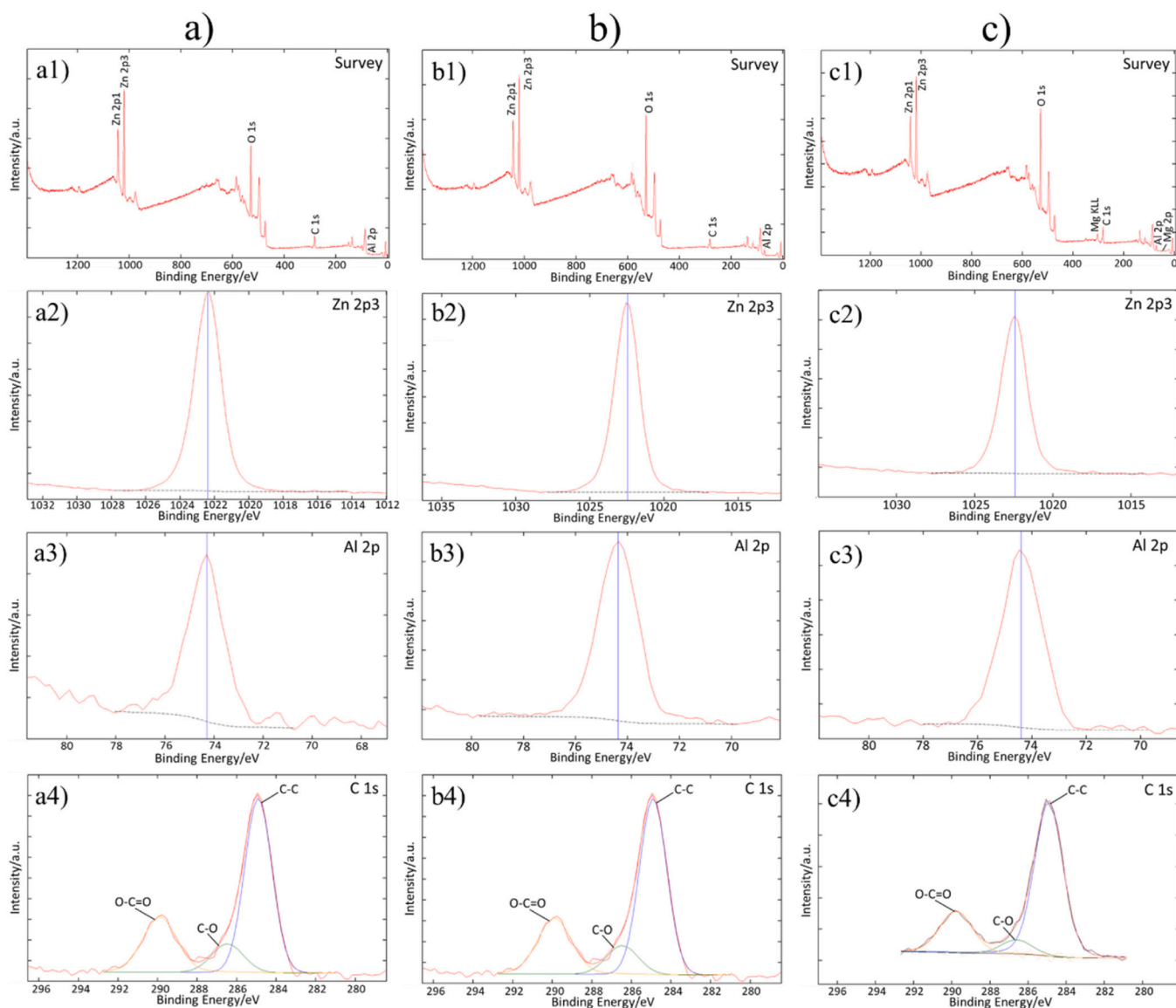


Fig. 8. Survey and high resolution XPS spectra of the HT-HDG (a), HT-ZA (b), and HT-ZAM (c) films after exposure to 0.1 M NaCl for 24 h.

which indicated that the chloride-containing corrosion products were not present on the extreme surface of HT film's samples. Compared with the original HT films, the twin peaks at around 1022.0 and 1045.0 eV of Zn 2p and at about 74.3 eV of Al 2p did not present significant changes, confirming that the Zn–Al HT films still exist on all the substrate

surfaces after immersion [36]. However, the decrease in the C 1s peaks for all the HT films present the lower amount of carbon atoms than these original samples and confirmed a partially removal of carbon ion. Moreover, the peaks of Mg 2p (50.0 eV) and Mg KLL Auger (300.0 eV), corresponding to corrosion products of the Mg such as MgO, Mg(OH)₂,

and MgCO_3 , were detected on the HT-ZAM surface (Fig. 8.c) [2]. The amount of corrosion products of the Mg oxidized on the HT-ZAM surface can be very small, therefore, they cannot be detected by XRD.

The morphology of all the substrates without and with HT films after 24 h of exposure to 0.1 M NaCl is shown in Fig. 9. It can be noted that a heterogeneous simonkolleite corrosion products layer was formed on the bare HDG surface, while the bare ZA and ZAM surfaces were covered by continuous Zn-Al- CO_3 HT nanosheets after 24 h. The morphology of all the Zn-Al HT films previously formed remained intact with nanoplates structure, however, only a small amount of HT nanoplates was dissolved, meaning that the Zn-Al HT films had a good adhesion to all the zinc coated steel substrates. Moreover, the HT-HDG film is partially covered by ZnO crystallites due to the partial dissolution of Zn-Al HT film and dissolution of the zinc alloy substrate (Fig. 9. a) [27,39]. A certain amount of ZnO precipitates can also be observed on the HT-ZA and HT-ZAM HT films but significantly less than on the HT-HDG film. Comparing the Zn-Al HT films formed on the bare ZA and ZAM substrates during immersion in the sodium chloride solution, the HT-ZA films previously synthesized were more uniform and denser, which can allow to avoid this substrate to be exposed to chloride ions and inhibit the corrosion process, while some gaps can be observed on the HT-ZAM film.

The chemical compositions of corrosion products of all the substrates without and with HT film were analyzed by EDS spectra and EDS maps after 24 h immersion (Table 4 and Fig. 10). The corrosion products formed on the bare HDG surface mainly contained Zn, Cl, C, and O elements, which can support the formation of simonkolleite. Besides, some regions enriched in Cl^- were observed with high intensity of Zn and O, confirming the co-existence of zincite and simonkolleite at the corroded sites (Fig. 10.a). In contrast, the detection of Zn, Al, C, and O elements on the bare ZA and ZAM surfaces indicated the existence of Zn-Al- CO_3 HT (Fig. 10.c and e). Similarly to HT 5/3 on EG steel sample [27], the uneven distribution of the Zn, Al, and O elements can be observed on the surface of the HT films on all zinc coated steel samples (Fig. 10.b, d, and f). For all HT film samples, the regions enriched in Al were also detected with higher intensity of O, proving that the HT nanoplates were not uniformly distributed (Fig. 10.b, d, f). The Al content of all HT film samples were significantly higher than those of the bare substrates after 24 h of immersion (Table 4). Moreover, the distribution of Al element on

Table 4

Element contents obtained from the EDS results of the HDG, ZA, and ZAM substrates without and with Zn-Al HT film after exposure to 0.1 M NaCl for 24 h.

Sample	Element content (wt%)					
	Zn	Al	O	C	Cl	Mg
HDG	69.8	0.8	25.0	2.7	1.1	–
HT-HDG 3	42.1	7.9	45.2	3.4	0.2	–
HT-HDG 4	65.1	4.5	28.2	1.9	0.2	–
ZA	76.1	4.4	17.7	1.8	0.2	–
HT-ZA 3	40.1	10.3	46.5	2.3	0.2	–
HT-ZA 4	65.2	5.6	27.2	1.9	0.1	–
ZAM	74.0	3.2	18.9	2.2	0.1	1.4
HT-ZAM 3	44.7	6.9	43.7	2.5	0.2	1.2
HT-ZAM 4	70.1	4.3	21.2	1.7	0.1	2.5

all the HT films was higher than those of bare substrates (Fig. 10), combining with the intensity of the characteristic peaks of Zn-Al- CO_3 HT crystallites from the XRD analysis, the thicknesses of as-prepared HT films on all the substrates was considerably higher than those of the HT produced due to corrosion in sodium chloride solution of the substrates containing Zn and Al in their composition. The O content of all samples increased significantly after immersion in NaCl solution, confirming the formation of the corrosion products containing O such as the oxidized Zn or Mg, simonkolleite, and HT on all the surfaces. Moreover, the presence of Cl elements can be observed on all the HT films surfaces after corrosion process, indicating that the HT films on all the substrates absorbed Cl^- ions of the corrosive solution and hold Cl^- ions in their positively charged layers [27].

3.3. Corrosion resistance of the Zn-Al HT conversion films on different zinc alloys coated steel substrates

The OCP stability of all the substrate samples without and with HT film was checked for 24 h in 0.1 M NaCl (Fig. 11). The OCP of the bare HDG and ZA substrates was divided into two different regions during immersion time. In the first 6 h of the surveyed period, the OCP values decreased and fluctuated, which was mainly due to the dissolution of the top layer of these substrates. However, the OCP values were stabilized at around -1.06 and -1.04 V versus Ag/AgCl for HDG and ZA substrates

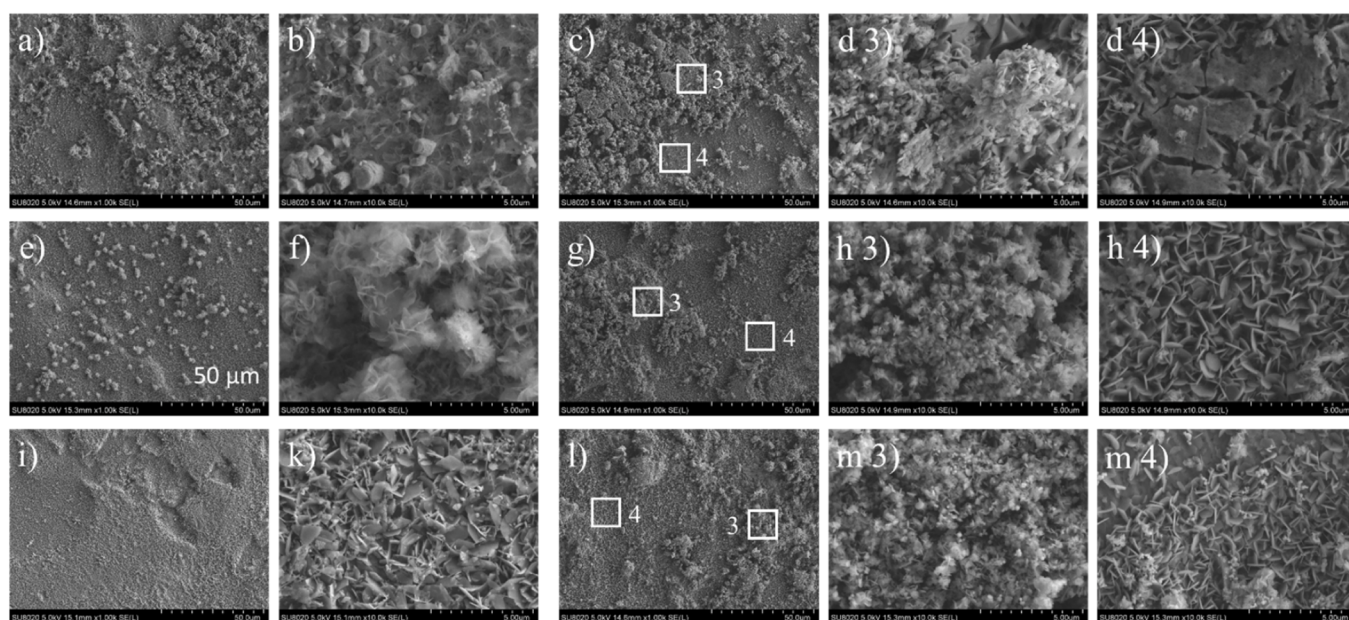


Fig. 9. SEM images of the HDG (a, b), HT-HDG (c, d3, d4), ZA (e, f), HT-ZA (g, h3, h4), ZAM (i, k), and HT-ZAM (l, m3, m4) samples after exposure to 0.1 M NaCl for 24 h.

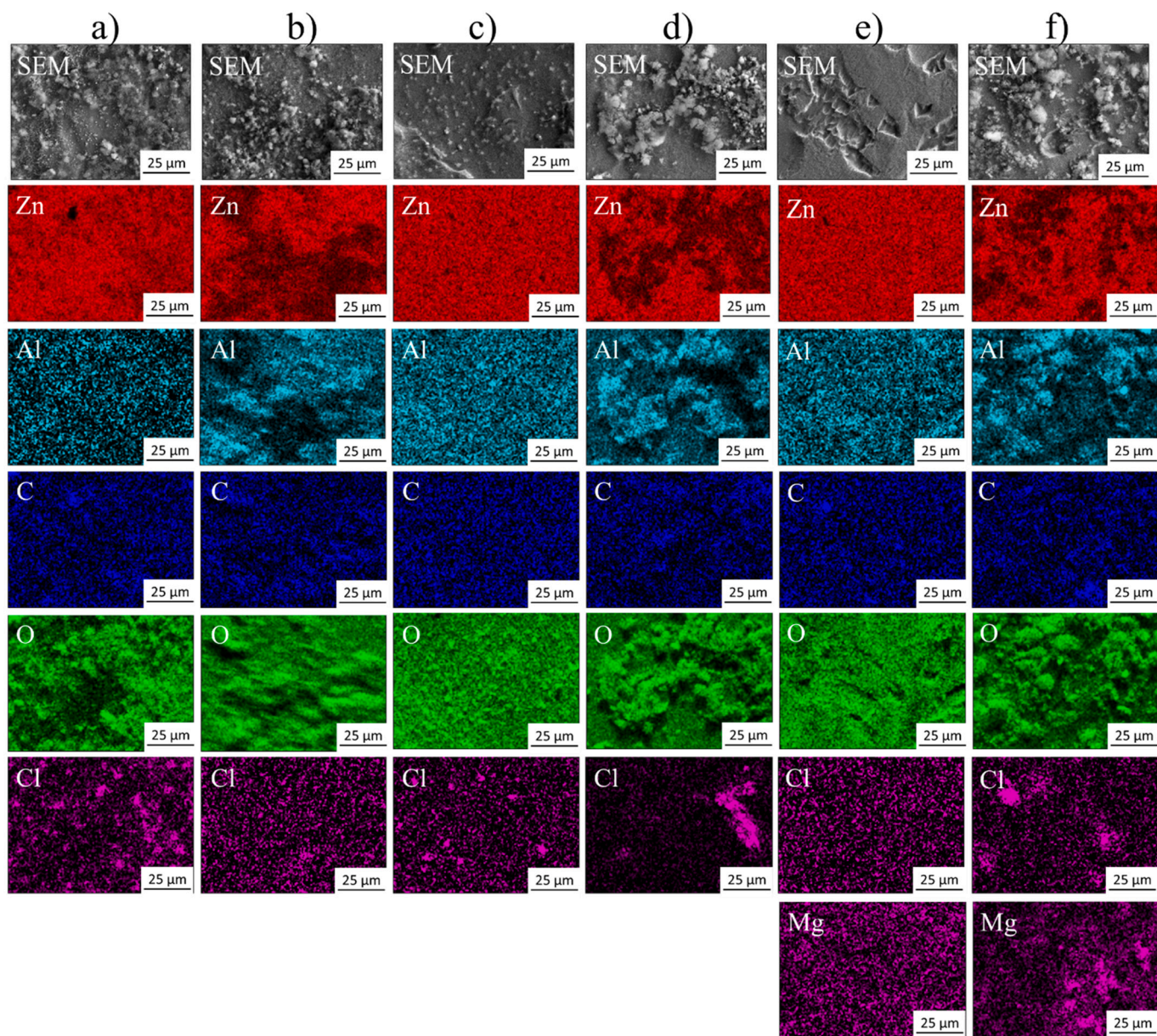


Fig. 10. EDS maps of the surface of HDG (a), HT-HDG (b), ZA (c), HT-ZA (d), ZAM (e), and HT-ZAM (f) samples after exposure to 0.1 M NaCl for 24 h.

in the remainder of immersion time, which confirmed the beginning of formation and deposition of corrosion products on these surfaces, leading to a slowdown of the substrate dissolution. The OCP values of the bare ZAM substrate was slightly lower during the first 6 h of immersion. However, these values increased sharply after 16 h of immersion, before remaining stable around -1.02 V versus Ag/AgCl. Compared with the bare HDG and ZA substrates, the OCP values of the bare ZAM substrate were more positive, which was representative of an anodic inhibitor with immersion time. The OCP values of all substrates with HT films were more positive and more stable than those of the bare substrates. Besides, the OCP values of the HT-HDG, HT-ZA, and HT-ZAM samples were stabilized at about -1.01 , -0.99 , and -0.95 V versus Ag/AgCl with immersion time, respectively.

The OCP values (Fig. 11) confirmed that HT films give an anodic protection for the substrates, therefore, the anodic polarization curves were used to evaluate the corrosion resistance of all the substrates without and with HT films. Fig. 12 presents the anodic polarization curves of the HDG, ZA, and ZAM substrates and HT film-coated samples, which were immersed in 0.1 M NaCl solution during a 24 h period. The

results of corrosion potential (E_{corr}), corrosion current densities (i_{corr}), and the anodic Tafel slopes (b_a) of all samples were listed in Table 5. The E_{corr} values of the bare HDG, ZA, and ZAM substrates were -1.06 ± 0.05 , -1.05 ± 0.03 , and -1.03 ± 0.06 V (vs. Ag/AgCl) respectively, while these values of the HT film-coated HDG, ZA, and ZAM samples were improved up to -1.00 ± 0.04 , -0.96 ± 0.07 , and -0.94 ± 0.05 V (vs. Ag/AgCl), respectively (Table 5). In comparison with the b_a values of all the bare substrates, these values of HT-HDG, HT-ZA, and HT-ZAM samples increased significantly, which implies that the HT films can block the anodic zones and hinder the anodic reaction [40]. This result led to an obvious decrease in corrosion current density of all HT films compared with bare substrates (Table 5). The decrease of i_{corr} values implied that the corrosion resistance of all the substrates was significantly enhanced with the HT film-coated, which was mainly due to the effective inhibition of the penetration of chlorides ions into the HT films.

The EIS was used to study the corrosion resistance and corrosion protection mechanism of the bare substrates and HT films during immersion in 0.1 M NaCl (Fig. 13 and Table 6). The impedance diagrams were fitted by electrochemical equivalent circuit (EEC) to clarify the

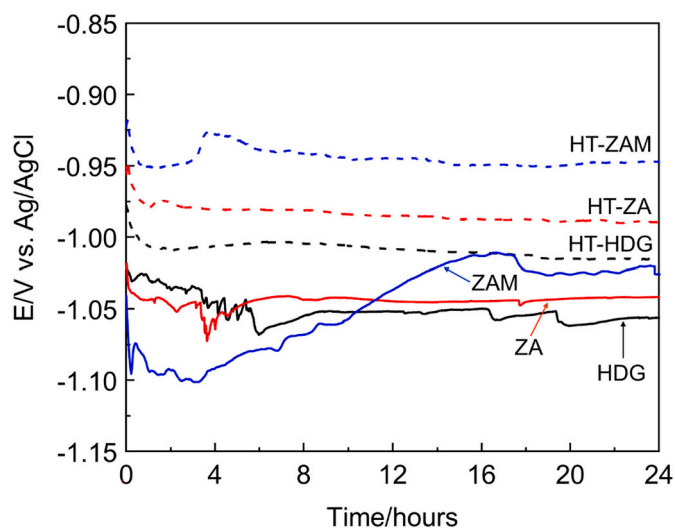


Fig. 11. The open circuit potential (OCP) of the HDG, ZA and ZAM substrates without and with Zn–Al HT films immersed in 0.1 M NaCl.

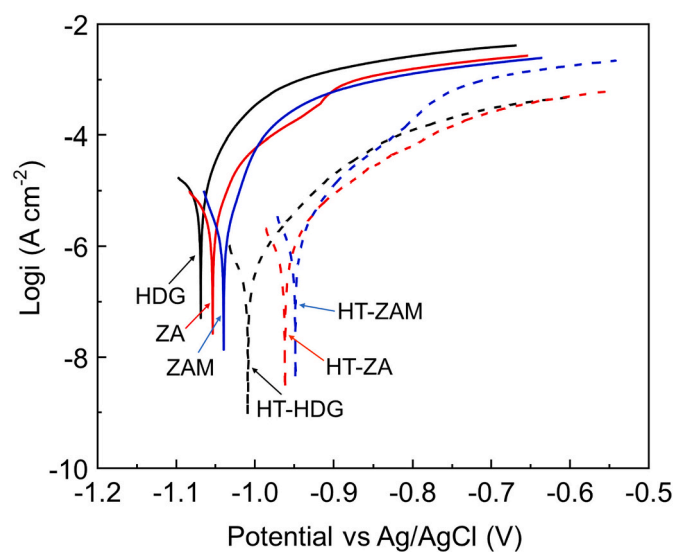


Fig. 12. Potentiodynamic polarization curves in 0.1 M NaCl of the HDG, ZA and ZAM substrates without and with Zn–Al HT films.

Table 5

The corrosion potential (E_{corr}), the corrosion current density (i_{corr}), and the anodic Tafel slopes (b_a) derived from the polarization measurement of the HDG, ZA, and ZAM substrates without and with HT film after exposure to 0.1 M NaCl for 24 h.

Samples	E_{corr} (V / Ag/AgCl)	i_{corr} ($\mu\text{A}\cdot\text{cm}^{-2}$)	b_a (mV $\cdot\text{dec}^{-1}$)
HDG	-1.06 ± 0.05	2.40 ± 0.04	44
HT-HDG	-1.00 ± 0.04	0.17 ± 0.01	82
ZA	-1.05 ± 0.03	2.00 ± 0.03	65
HT-ZA	-0.96 ± 0.07	0.25 ± 0.02	94
ZAM	-1.03 ± 0.06	1.81 ± 0.03	39
HT-ZAM	-0.94 ± 0.05	0.41 ± 0.02	76

anti-corrosion behavior of the bare substrates and HT films (Fig. 14). The structural characteristics results of all samples before and after exposure to 0.1 M NaCl showed the film heterogeneity. Therefore, to reflect the heterogeneity of the composition, the constant phase element (CPE) was used as a substitute for pure capacitance (C). The relationship between CPE and C was calculated by $C = \text{CPE} (\omega_{\text{max}})^{n-1}$, where the CPE

and n parameters are used to describe the electrode's response [41]. The impedance diagrams of all the bare substrates clearly presented two time constants after 2 h, thus the model $R_s(\text{CPE}_{f1}(R_{f1}(\text{CPE}_{dl}R_p)))$, where R_s was the solution resistance, R_{f1} and CPE_{f1} were representative of the outer film, and R_p and CPE_{dl} were related to the double layer, was used for the EIS fitting results (Fig. 14.a). The first time constant seen in the medium frequency region, was related to the outer films composed by the Zn, Al, and Mg oxides/hydroxides [27]. The R_{f1} values of the HDG, ZA, and ZAM substrates after 2 h of immersion were 1167, 1366, and $1578 \Omega\cdot\text{cm}^2$, respectively, indicating that the barrier properties of those films were relatively similar. The second time constant associated with the electrochemical process of all the bare substrates at the interface can be observed in the low frequency regions after 2 h. The R_p values of the HDG, ZA, and ZAM gained 1184, 1862, and $4948 \Omega\cdot\text{cm}^2$, respectively, confirming that the corrosion protection of ZAM substrate was sharply higher than those of the other two substrates. The two time constants were also observed for the ZA and ZAM substrates after 24 h of immersion and the same EEC was used ($\text{CPE}_{f1}(R_{f1}(\text{CPE}_{dl}R_p))$) (Fig. 14.a). Combining with the results from XRD, XPS, SEM/EDS analysis after 24 h of those samples, the R_{f1} and CPE_{f1} were related to the Zn–Al– CO_3 HT corrosion product film. The R_p values of the ZA and ZAM substrates reduced after 24 h, indicating a decrease of the corrosion protection of those samples. However, there was only one time constant for the HDG substrate after 24 h, which indicated that the corrosion products merged into one layer [27]. The fitted model $R_s(\text{CPE}_{dl}R_p)$ was selected for the HDG substrate after a exposure time of 24 h (Fig. 14.b).

The electrochemical impedance diagrams of HT-HDG and HT-ZA samples showed three time constants in the given period, therefore, the model $R_s(\text{CPE}_{f1}(R_{f1}(\text{CPE}_{f2}(R_{f2}(\text{CPE}_{dl}R_p))))$ was suitable for the EIS results (Fig. 14.c). Combining with structural and surface analysis results, the R_s was the solution resistance, R_{f1} and CPE_{f1} were related to the oxide film, R_{f2} and CPE_{f2} were representative of the electrochemical behavior of the Zn–Al– CO_3 HT film and, finally R_p and CPE_{dl} were associated with the double layer. In contrast, two time constants can be observed from the HT-ZAM impedance diagrams during the exposure time. The fitted model $R_s(\text{CPE}_{f1}(R_{f1}(\text{CPE}_{dl}R_p)))$, where R_{f1} and CPE_{f1} were related to the Zn–Al– CO_3 HT film and, R_p and CPE_{dl} to the double layer (Fig. 14.a). The previous works showed that the dissolution of the Mg from ZAM substrates buffered the pH at cathodic regions inhibiting the ZnO formation [4,42,43]. Therefore, the amount of ZnO and MgO crystallites formed on HT-ZAM surfaces was very small and there was not time constant of the oxide film in the HT-ZAM impedance diagrams, which completely matched the corrosion product results of HT-ZAM sample. The HT-HDG R_{oxide} values showed an upward trend from 182 to $489 \Omega\cdot\text{cm}^2$, while those of HT-ZA showed a downward trend from 167 to $98 \Omega\cdot\text{cm}^2$. Although these oxide film's barrier properties were relatively low, they can affect the stability of the HT films and double layer [27]. After 2 h, the HT-ZA CPE_{HT} value ($2.34 \times 10^{-5} \Omega^{-1}\cdot\text{s}^n\cdot\text{cm}^{-2}$), was not much different from the HT-HDG CPE_{HT} value ($3.68 \times 10^{-5} \Omega^{-1}\cdot\text{s}^n\cdot\text{cm}^{-2}$), which significantly lower than that of HT-ZAM sample ($8.89 \times 10^{-5} \Omega^{-1}\cdot\text{s}^n\cdot\text{cm}^{-2}$). The lower CPE_{HT} values of HT-ZA and HT-HDG confirmed the relatively denser HT film formed in these substrates. The CPE_{HT} value of all HT films rose after 24 h (Table 6), showing that the exposure of HT films with porous structure to electrolyte solution reduced their compactness. The HT-ZA R_{HT} value was $6240 \Omega\cdot\text{cm}^2$ after immersion of 2 h, which was considerably higher than those of HT-HDG ($4803 \Omega\cdot\text{cm}^2$) and HT-ZAM ($4589 \Omega\cdot\text{cm}^2$) samples (Table 6). However, this value of HT 5/3 on EG steel ($8681 \Omega\cdot\text{cm}^2$) in our previous study was slightly higher than that of HT-ZA [27]. This can be explained by the fact that the thickness of HT-ZA and HT 5/3 films was larger than those of other two HT films (Fig. 6). Similarly with HT 5/3 sample [27], the HT-HDG, HT-ZA, and HT-ZAM R_{HT} values reduced to $4087 \Omega\cdot\text{cm}^2$, $3522 \Omega\cdot\text{cm}^2$, and $4411 \Omega\cdot\text{cm}^2$, respectively, after 24 h. Because these HT films were porous, the aggressive species as Cl^- can easily penetrate and destroy them. Besides, comparing with the R_{HT} values of the HT corrosion product film on ZA and ZAM, the HT-ZA and

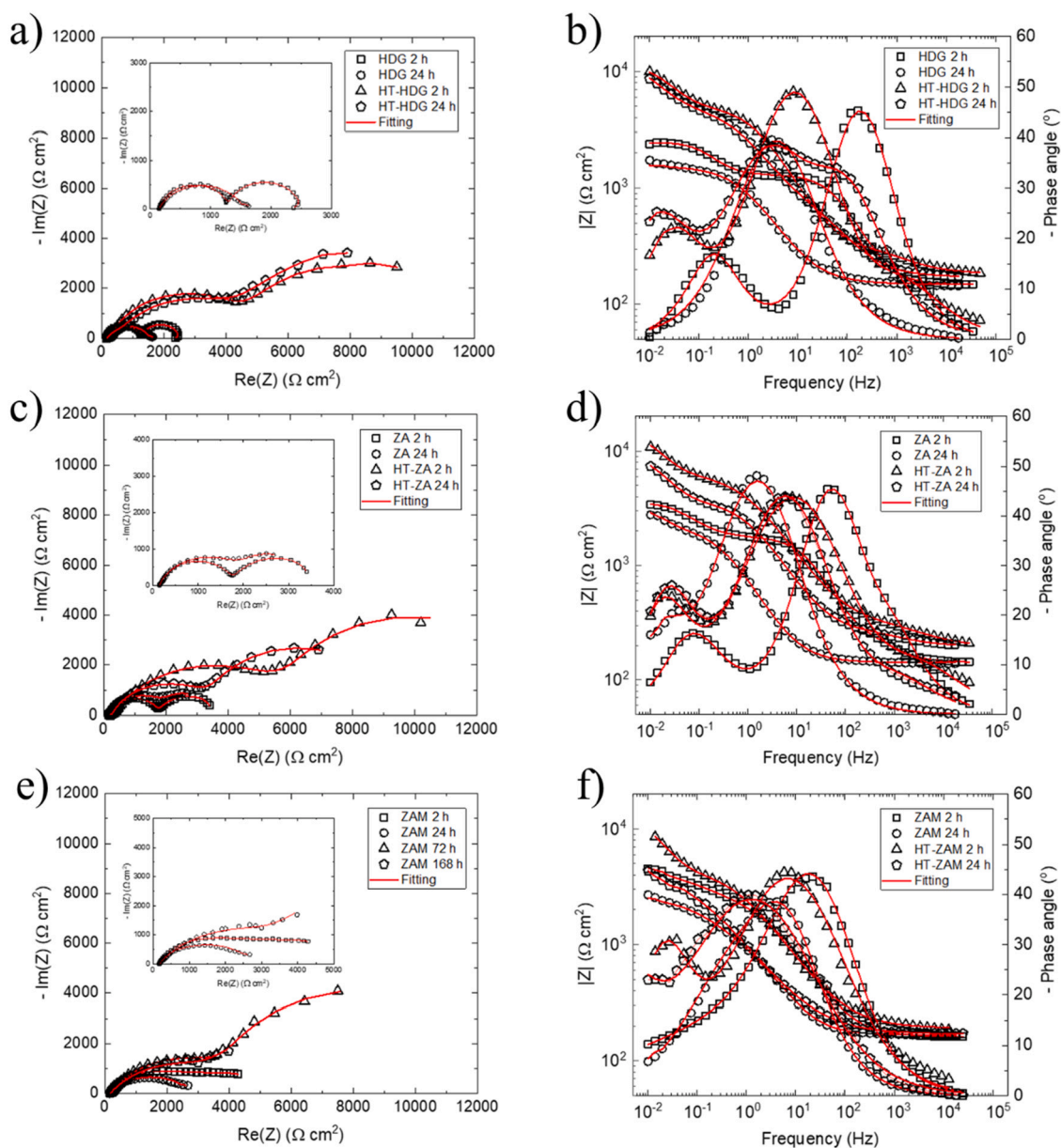


Fig. 13. Nyquist and bode plots of the HDG and HT-HDG (a, b), the ZA and HT-ZA (c, d); and the ZAM and HT-ZAM (e, f) samples.

Table 6

Parameters of EIS for all samples after exposure to 0.1 M NaCl.

Samples	$CPE_{R1} (\Omega^{-1} \cdot s^n \cdot cm^{-2})$	n_{R1}	$R_{R1} (\Omega \cdot cm^2)$	$CPE_{R2} (\Omega^{-1} \cdot s^n \cdot cm^{-2})$	n_{R2}	$R_{R2} (\Omega \cdot cm^2)$	$CPE_{dl} (\Omega^{-1} \cdot s^n \cdot cm^{-2})$	n	$R_p (\Omega \cdot cm^2)$	$ Z _{10 \text{ mHz}} (\Omega \cdot cm^2)$
HDG-2 h	5.66×10^{-6}	0.89	1167				9.89×10^{-4}	0.94	1184	2378
HDG-24 h							2.31×10^{-4}	0.76	1409	1738
HT-HDG-2 h	1.89×10^{-5}	0.7	182	2.34×10^{-5}	0.85	4803	1.08×10^{-3}	0.75	6071	9927
HT-HDG-24 h	3.01×10^{-5}	0.74	489	7.24×10^{-5}	0.75	4087	1.32×10^{-3}	0.83	8777	8615
ZA-2 h	1.09×10^{-5}	0.78	1366				1.49×10^{-3}	0.84	1862	3419
ZA-24 h	3.23×10^{-4}	0.8	2072				7.59×10^{-3}	0.9	1430	2773
HT-ZA-2 h	1.31×10^{-5}	0.66	167	3.68×10^{-5}	0.76	6240	1.38×10^{-3}	0.91	7837	10,433
HT-ZA-24 h	2.08×10^{-5}	0.74	98	5.47×10^{-5}	0.77	3522	1.70×10^{-3}	0.93	5528	7386
ZAM-2 h	4.42×10^{-5}	0.78	1578				4.65×10^{-4}	0.62	4948	4351
ZAM-24 h	1.75×10^{-4}	0.8	985				6.67×10^{-4}	0.6	1513	2691
HT-ZAM-2 h	8.89×10^{-5}	0.68	4589				1.24×10^{-3}	0.95	8294	9526
HT-ZAM-24 h	3.46×10^{-4}	0.61	4411				3.52×10^{-3}	0.92	4789	4319

HT-ZAM R_{HT} values were sharply higher, conforming that their barrier properties were better. Due to HT films formation at a high pH solution, the HT nucleation process led to Zn^{2+} and Al^{3+} dissolution on the top

surface of substrates. Therefore, the surface of zinc alloy substrates presented cavity and hole morphology under the HT films [26], which caused higher HT film CPE_{dl} values compared to those of bare substrates

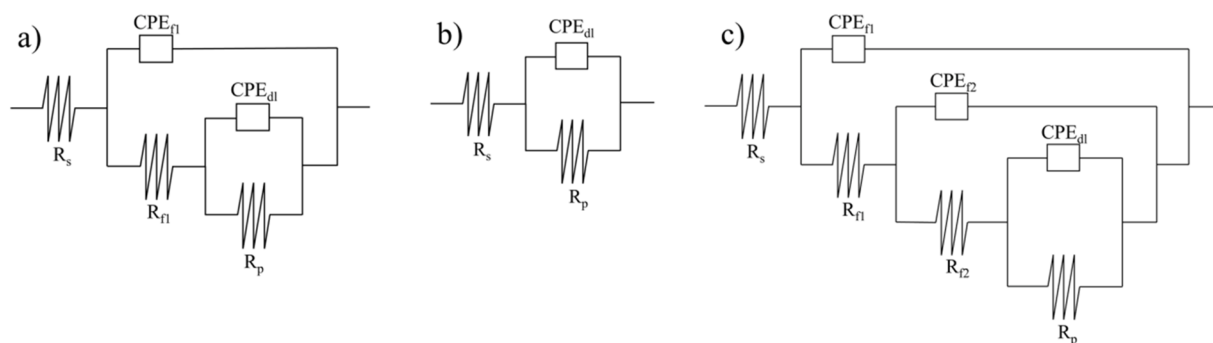
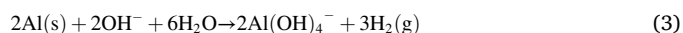


Fig. 14. Electrochemical equivalent circuit for the EIS data fitting of bare substrates and Zn–Al HT films.

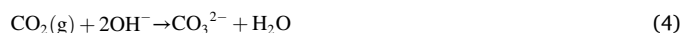
during immersion time (Table 6). However, the CPE_{dl} value of all HT films increased slightly after 24 h (Table 6). This can be explained by the dense packing of HT films, which decreased the migration of Cl^- anions to the underlying zinc alloy coatings. The impedance modulus value at 10 mHz ($|Z|_{10\text{ mHz}}$) and R_p values of all HT films were considerably higher than those of bare substrates (Table 6), suggesting that the corrosion resistance of the substrates coated with HT films was enhanced significantly [13]. The HT-HDG R_p values raised from 6071 to 8777 $\Omega\cdot\text{cm}^2$, while the HT-ZA and HT-ZAM R_p values reduced sharply from 7837 to 5528 $\Omega\cdot\text{cm}^2$ and from 8294 to 4789 $\Omega\cdot\text{cm}^2$. The HT-HDG R_{oxide} value after 24 h was sharply higher than that of HT-ZA samples, confirming the large amount of ZnO crystallites formed by recrystallization of Zn^{2+} ions. These ZnO crystallites sealed the damaged areas of HT-HDG film and HDG surface substrate, as observed from the SEM analysis results (Fig. 9). In contrast, it was observed that the small amount of ZnO crystallites was precipitated on the HT-ZA and HT-ZAM surfaces, which cannot seal and repair the damaged areas (Fig. 9). Therefore, the HT-HDG was significantly more effective against corrosion by Cl^- ions and acquired better performance.

3.4. Discussion

From the characterization and surface morphology results, the mechanism of Zn-Al- CO_3^{2-} HT growth process can be proposed (Fig. 15). The zinc and aluminum metals can be active in the high pH solutions. In contrast, magnesium metal did not participate in the HT growth process. Therefore, the zinc alloys containing aluminum provided Zn^{2+} and Al^{3+} from the dissolution of the substrates in the pH 12 solution [14,26]:



The CO_2 dissolution from the air provided CO_3^{2-} anions [26]:



The $Zn(NO_3)_2$ and $Al(NO_3)_3$ salts added to the reaction mixture also provided $Zn(OH)_3^-$ and $Al(OH)_4^-$ for HT film formation [27]:

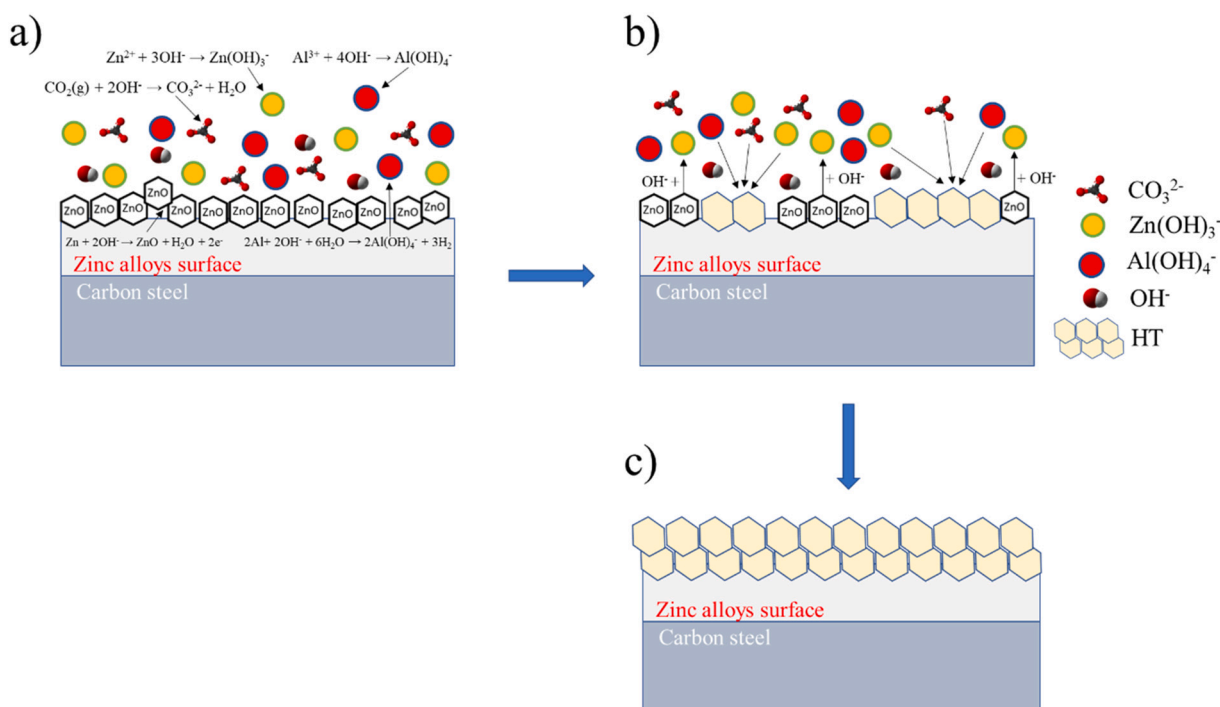
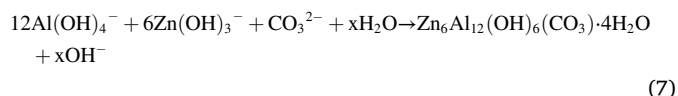


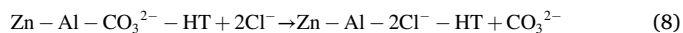
Fig. 15. The mechanism of HT growth process on HDG, ZA and ZAM substrates. Dissolution of the substrates and formation of ZnO (a), HT nucleation process (b), and HT deposition on substrate surfaces.



The elemental compositions and roughness of the zinc coated steel substrates showed insignificant influence on the chemical compositions and structure of the Zn–Al HT films. However, they significantly affected the deposition of HT crystallites on these substrates, which were expressed in morphology, thickness, and porosity differences of HT films.

Fig. 16 presented the schematic representation of the corrosion protection of Zn–Al HT films on the HDG, ZA and ZAM substrates in 0.1 M NaCl solution. In the aggressive environments containing Cl^- ions, the dense HT coated-films played a physical protective layer, which isolated Cl^- ions and the zinc coated steel substrates (Fig. 16.a) [44]. On exposure with corrosion anions, the HT coated-films started exchange of CO_3^{2-} ions with Cl^- ions, thus these Cl^- ions were captured and restricted to move in the HT interlayer (Fig. 16.b) [19,27]. Therefore,

the HT films decreased the possibility of Cl^- coming into contact with the zinc coated steel substrates and impeded the corrosion of these substrates. The ion-exchange reaction of the HT coated-films on all the zinc coated steel substrates in the aggressive environments containing Cl^- ions was given as follows [27]:



Besides, when a small amount of Cl^- ions passed through the HT interlayer and reacted with top layer of these substrate, the pH and ion contents in the solution near these areas were changed. The HT crystallites were cracked and partially destroyed under the stress, releasing Zn^{2+} and Al^{3+} ions (Fig. 16.c1 and c2) [39]. From XPS results (Fig. 8.c), the dissolution of the ZAM coating at the corroded sites provided Mg^{2+} cations (Fig. 16.c2), which led to the formation of Mg oxidized corrosion products and interfered with the formation of ZnO [4]. Then the ZnO crystallites formed on the corrosion cracking zone of HT-HDG and HT-ZA due to self-healing effect, healing the corrosion pits and providing the protective layer (Fig. 16.d1). In contrast, the ZnO and MgO formation on HT-ZAM samples was not enough to provide the oxide layer on HT film (Fig. 16.d2).

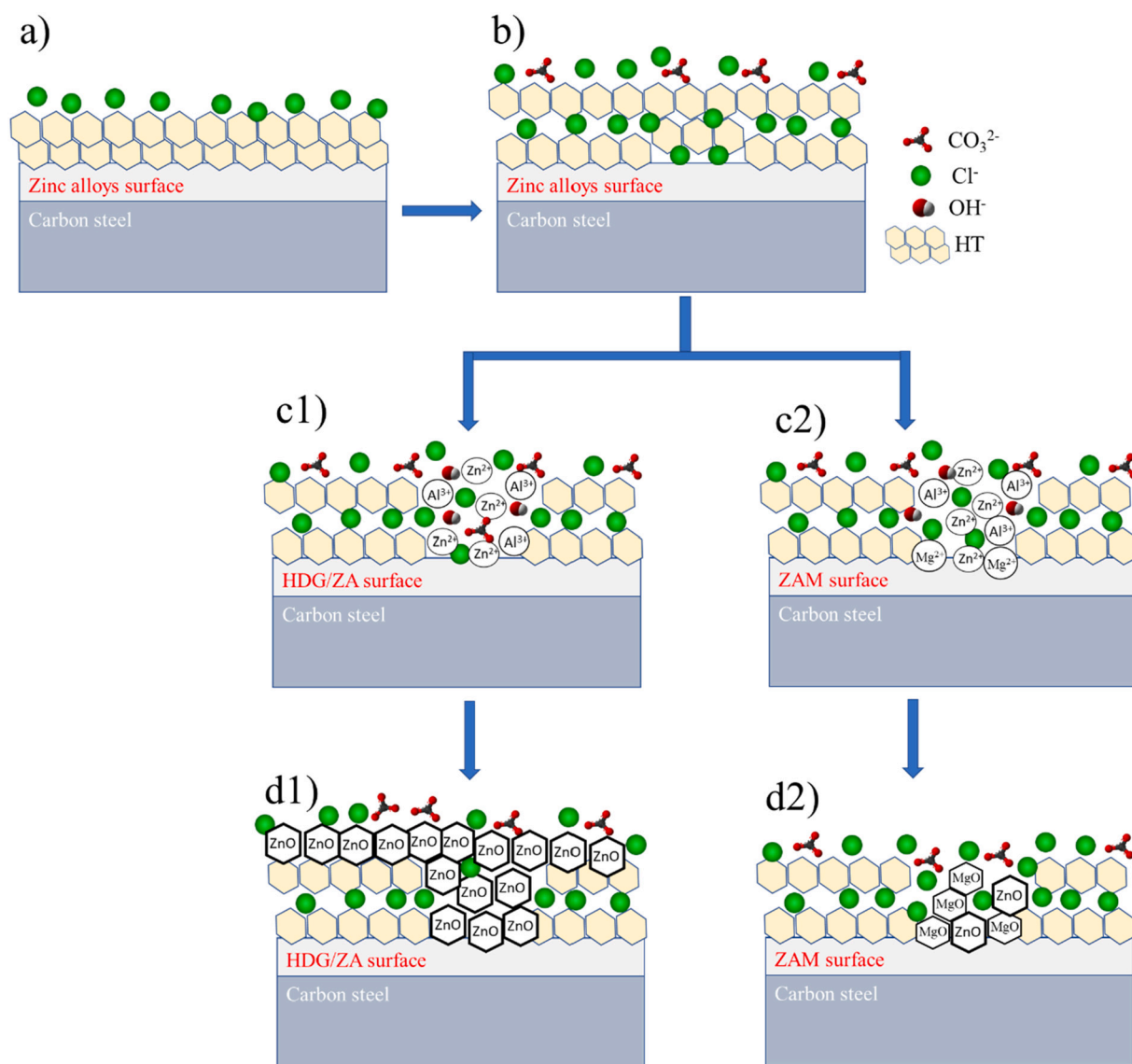


Fig. 16. Corrosion protection mechanism of the Zn–Al HT film-coated samples. HT played a physical protective layer (a), ion exchange between CO_3^{2-} and Cl^- in the HT interlayer (b), partial destruction of HT crystallites and top layer of substrates under the stress and releasing Zn^{2+} , Al^{3+} , and/or Mg^{2+} cations (c1 and c2), metal oxides formation on HT surfaces (d1 and d2).

4. Conclusions

The Zn–Al HT intercalated with carbonate anions films were successfully developed on the different zinc alloys coated steel at room temperature and pH 12. These results presented that the changes of compositions and roughness of the zinc coated steel substrates did not affect the HT film's structure, however, they had notable effects on the morphology, thickness, porosity, and corrosion resistance behavior of these films. Comparing with the bare zinc alloys substrates, the samples covered by HT films showed a considerably enhanced anti-corrosion during exposure time in a sodium chloride solution. Moreover, the HT-HDG samples retained the anti-corrosion, while the corrosion protection of HT-ZA and HT-ZAM was reduced with immersion for 24 h. The inhibitive effect of HT films can be elucidated from main factors: the physical protective layer and the ion-exchange and competitive adsorption for Cl^- ions. Moreover, the corrosion protection of HT-HDG and HT-ZA can be affected by the deposition of ZnO on the HT films and corrosion zones. For the case of HT-ZAM, the formation of Mg oxidized corrosion products interfered with the formation of ZnO at the interface.

Declaration of competing interest

The Université de Mons has received a financial funding coming from the ARES (Belgium) in the framework of the PRD Project "RENFORCEMENT DE L'EXPERTISE ENVIRONNEMENTALE DU CENTRE DE COMPÉTENCES EN PROTECTION CONTRE LA CORROSION ET EN ÉLECTROCHIMIE", Institute of Tropical Technology, Vietnam", 2020–2025.

This project attributed a PhD grant to Pham Thu Thuy for coming in Belgium for a part of her research (six months per year).

Data availability

No data was used for the research described in the article.

Acknowledgments

The authors would like to thank ArcelorMittal for providing the metallic substrate and Sebastien Colmant from Metallurgy Department for his help to prepare the embedded samples. This study was supported by the Académie de Recherche et d'Enseignement Supérieur (ARES Belgium) through the Development Cooperation project between Vietnam and Belgium (PRD 2020-2025: Renforcement de l'expertise environnementale du centre de compétences en protection contre la corrosion et en électrochimie).

References

- Y. Meng, L. Liu, D. Zhang, C. Dong, Y. Yan, A.A. Volinsky, L.N. Wang, Initial formation of corrosion products on pure zinc in saline solution, *Bioact. Mater.* 4 (2019) 87–96.
- J. Rodriguez, L. Chenoy, A. Roobroeck, S. Godet, M.G. Olivier, Effect of the electrolyte pH on the corrosion mechanisms of zn-mg coated steel, *Corros. Sci.* 108 (2016) 47–59.
- F. Andreatta, J. Rodriguez, M. Mouanga, A. Lanzutti, L. Fedrizzi, M.G. Olivier, Corrosion protection by zinc-magnesium coatings on steel studied by electrochemical methods, *Mater. Corros.* 70 (2018) 793–801.
- D. Persson, D. Thierry, N. LeBozec, T. Prosek, In situ infrared reflection spectroscopy studies of the initial atmospheric corrosion of Zn–Al–Mg coated steel, *Corros. Sci.* 72 (2013) 54–63.
- M. Salgueiro Azevedo, C. Allély, K. Ogle, P. Volovitch, Corrosion mechanisms of Zn (Mg, Al) coated steel in accelerated tests and natural exposure: 1. The role of electrolyte composition in the nature of corrosion products and relative corrosion rate, *Corros. Sci.* 90 (2015) 472–481.
- D. Nguyen Thuy, H. To Thi Xuan, A. Nicolay, Y. Paint, M.-G. Olivier, Corrosion protection of carbon steel by solvent free epoxy coating containing hydrotalcites intercalated with different organic corrosion inhibitors, *Prog. Org. Coat.* 101 (2016) 331–341.
- D.T. Nguyen, H.T.X. To, J. Gervasi, Y. Paint, M. Gonon, M.-G. Olivier, Corrosion inhibition of carbon steel by hydrotalcites modified with different organic carboxylic acids for organic coatings, *Prog. Org. Coat.* 124 (2018) 256–266.
- J. Rodriguez, E. Bollen, T.D. Nguyen, A. Portier, Y. Paint, M.G. Olivier, Incorporation of layered double hydroxides modified with benzotriazole into an epoxy resin for the corrosion protection of zn-mg coated steel, *Prog. Org. Coat.* 149 (2020), 105894.
- Y. Su, S. Qiu, J. Wei, X. Zhu, H. Zhao, Q. Xue, Sulfonated polyaniline assisted hierarchical assembly of graphene-LDH nanohybrid for enhanced anticorrosion performance of waterborne epoxy coatings, *Chem. Eng. J.* 426 (2021), 131269.
- A. Collazo, M. Hernández, X.R. Nóvoa, C. Pérez, Effect of the addition of thermally activated hydrotalcite on the protective features of sol–gel coatings applied on AA2024 aluminium alloys, *Electrochim. Acta* 56 (2011) 7805–7814.
- D. Álvarez, A. Collazo, M. Hernández, X.R. Nóvoa, C. Pérez, Characterization of hybrid sol–gel coatings doped with hydrotalcite-like compounds to improve corrosion resistance of AA2024-T3 alloys, *Prog. Org. Coat.* 68 (2010) 91–99.
- Y. Zhang, P. Yu, J. Wu, F. Chen, Y. Li, Y. Zhang, Y. Zuo, Y. Qi, Enhancement of anticorrosion protection via inhibitor-loaded zn-AlCe-LDH nanocontainers embedded in sol–gel coatings, *J. Coat. Technol. Res.* 15 (2017) 303–313.
- Y. Tang, F. Wu, L. Fang, T. Guan, J. Hu, S. Zhang, A comparative study and optimization of corrosion resistance of zn-Al layered double hydroxides films intercalated with different anions on AZ31 mg alloys, *Surf. Coat. Technol.* 358 (2019) 594–603.
- F. Wang, Z. Guo, In situ growth of durable superhydrophobic Mg–Al layered double hydroxides nanoplatelets on aluminum alloys for corrosion resistance, *J. Alloys Compd.* 767 (2018) 382–391.
- R. Shi, P. Yang, Y. Yin, X. Dong, J. Li, Fabrication of porous microspheres and network arrays of Zn–Al hydrotalcite-like compounds on Al substrate via facile hydrothermal method, *Ceram. Int.* 40 (2014) 6855–6863.
- H. Chen, F. Zhang, S. Fu, X. Duan, In situ microstructure control of oriented layered double hydroxide monolayer films with curved hexagonal crystals as superhydrophobic materials, *Adv. Mater.* 18 (2006) 3089–3093.
- M.A. Iqbal, L. Sun, A.M. LaChance, H. Ding, M. Fedel, In situ growth of a CaAl-NO₃-layered double hydroxide film directly on an aluminum alloy for corrosion resistance, *Dalton Trans.* 49 (2020) 3956–3964.
- R.-C. Zeng, Z.-G. Liu, F. Zhang, S.-Q. Li, H.-Z. Cui, E.-H.J.J.O.M.C.A. Han, Corrosion of molybdate intercalated hydrotalcite coating on AZ31 Mg alloy, *J. Mater. Chem. A* 2 (2014) 13049–13057.
- F. Zhang, Z.-G. Liu, R.-C. Zeng, S.-Q. Li, H.-Z. Cui, E.-H. Han, Corrosion resistance of Mg–Al-LDH coating on magnesium alloy AZ31, *Surf. Coat. Technol.* 258 (2014) 1152–1158.
- R.-C. Zeng, X.-T. Li, Z.-G. Liu, F. Zhang, S.-Q. Li, H.-Z. Cui, Corrosion resistance of Zn–Al layered double hydroxide/poly(lactic acid) composite coating on magnesium alloy AZ31, *Front. Mater. Sci.* 9 (2015) 355–365.
- X. Wang, L. Li, Z.-H. Xie, G. Yu, Duplex coating combining layered double hydroxide and 8-quinolinol layers on mg alloy for corrosion protection, *Electrochim. Acta* 283 (2018) 1845–1857.
- A. Mikhailau, H. Maltanova, S.K. Poznyak, A.N. Salak, M.L. Zheludkevich, K. A. Yasakau, M.G.S. Ferreira, One-step synthesis and growth mechanism of nitrate intercalated zn-Al LDH conversion coatings on zinc, *Chem. Commun.* 55 (2019) 6878–6881.
- A.C. Bouali, M.H. Iuzviuk, M. Serdechnova, K.A. Yasakau, D.C.F. Wieland, G. Dovzhenko, H. Maltanova, I.A. Zobkalo, M.G.S. Ferreira, M.L. Zheludkevich, Zn-Al LDH growth on AA2024 and zinc and their intercalation with chloride: comparison of crystal structure and kinetics, *Appl. Surf. Sci.* 501 (2020), 144027.
- R. Buchheit, H. Guan, Formation and characteristics of Al-zn hydrotalcite coatings on galvanized steel, *J. Coat. Technol. Res.* 1 (2004) 277–290.
- K. Hoshino, S. Furuya, R.G. Buchheit, Effect of NO₃– intercalation on corrosion resistance of conversion coated zn-Al-CO₃ LDHs on electrogalvanized steel, *J. Electrochem. Soc.* 165 (2018) C461–C468.
- K. Hoshino, S. Furuya, R.G. Buchheit, Effect of solution pH on layered double hydroxide formation on electrogalvanized steel sheets, *J. Mater. Eng. Perform.* 28 (2019) 2237–2244.
- T.T. Pham, T.D. Nguyen, A.S. Nguyen, Y. Paint, M. Gonon, T.X.H. To, M.-G. Olivier, A comparative study of the structure and corrosion resistance of zn-Al hydrotalcite conversion layers at different Al³⁺/Zn²⁺ ratios on electrogalvanized steel, *Surf. Coat. Technol.* 429 (2022), 127948.
- J. Lin, C. Hsia, J. Uan, Characterization of mg, Al-hydrotalcite conversion film on mg alloy and Cl⁻ and CO₃²⁻ anion-exchangeability of the film in a corrosive environment, *Scr. Mater.* 56 (2007) 927–930.
- J. Lin, J. Uan, Formation of mg, Al-hydrotalcite conversion coating on mg alloy in aqueous HCO₃⁻/CO₃²⁻ and corresponding protection against corrosion by the coating, *Corros. Sci.* 51 (2009) 1181–1188.
- B.-L. Yu, J.-K. Lin, J.-Y. Uan, Applications of carbonic acid solution for developing conversion coatings on mg alloy, *Trans. Nonferrous Metals Soc. China* 20 (2010) 1331–1339.
- J. Chen, Y. Song, D. Shan, E.-H. Han, Study of the in situ growth mechanism of Mg–Al hydrotalcite conversion film on AZ31 magnesium alloy, *Corros. Sci.* 63 (2012) 148–158.
- J. Chen, Y. Song, D. Shan, E.-H. Han, In situ growth of Mg–Al hydrotalcite conversion film on AZ31 magnesium alloy, *Corros. Sci.* 53 (2011) 3281–3288.
- J. Kuang, Z. Ba, Z. Li, Y. Jia, Z. Wang, Fabrication of a superhydrophobic mg-mn layered double hydroxides coating on pure magnesium and its corrosion resistance, *Surf. Coat. Technol.* 361 (2019) 75–82.
- A.A.A. Ahmed, Z.A. Talib, M.Z. Bin Hussein, A. Zakaria, Zn–Al layered double hydroxide prepared at different molar ratios: preparation, characterization, optical and dielectric properties, *J. Solid State Chem.* 191 (2012) 271–278.

- [35] R. Comparelli, E. Fanizza, M. Curri, P. Cozzoli, G. Mascolo, A. Agostiano, UV-induced photocatalytic degradation of azo dyes by organic-capped ZnO nanocrystals immobilized onto substrates, *Appl. Catal., B* 60 (2005) 1–11.
- [36] Z. Li, M. Chen, H. Hu, Q. Zhang, D. Tao, Mechanochemical synthesis of novel pt modified zn-Al-LDH for effective ciprofloxacin photodegradation, *J. Solid State Chem.* 290 (2020), 121594.
- [37] W.-D. Zhang, Q.-T. Hu, L.-L. Wang, J. Gao, H.-Y. Zhu, X. Yan, Z.-G. Gu, In-situ generated ni-MOF/LDH heterostructures with abundant phase interfaces for enhanced oxygen evolution reaction, *Appl. Catal., B* 286 (2021), 119906.
- [38] C. Gomes, Z. Mir, R. Sampaio, A. Bastos, J. Tedim, F. Maia, C. Rocha, M. Ferreira, Use of zn-Al-layered double hydroxide (LDH) to extend the service life of reinforced concrete, *Materials (Basel)* 13 (2020) 1769.
- [39] T. Yan, S. Xu, Q. Peng, L. Zhao, X. Zhao, X. Lei, F. Zhang, Self-healing of layered double hydroxide film by dissolution/recrystallization for corrosion protection of aluminum, *J. Electrochem. Soc.* 160 (2013) C480.
- [40] G. Zhang, L. Wu, A. Tang, Y. Ma, G.-L. Song, D. Zheng, B. Jiang, A. Atrens, F. Pan, Active corrosion protection by a smart coating based on a MgAl-layered double hydroxide on a cerium-modified plasma electrolytic oxidation coating on mg alloy AZ31, *Corros. Sci.* 139 (2018) 370–382.
- [41] T.D. Nguyen, B.A. Tran, K.O. Vu, A.S. Nguyen, A.T. Trinh, G.V. Pham, T.X.H. To, M.V. Phan, T.T. Phan, Corrosion protection of carbon steel using hydrotalcite/graphene oxide nanohybrid, *J. Coat. Technol. Res.* 16 (2018) 585–595.
- [42] K. Nishimura, H. Shindo, K. Kato, Y. Morimoto, Microstructure and corrosion behaviour of Zn–Mg–Al hot-dip galvanized steel sheet, in: *Proceedings of the Galvatech '98, International Conference on Zinc and Zinc Alloy Coated Steel*, Chiba, Japan, September 20–23, 1998, pp. 437–442.
- [43] S. Schürz, G.H. Luckeneder, M. Fleischanderl, P. Mack, H. Gsaller, A.C. Kneissl, G. Mori, Chemistry of corrosion products on Zn–Al–Mg alloy coated steel, *Corros. Sci.* 52 (2010) 3271–3279.
- [44] G. Nikhil, R. Ji, Prakash, hydrothermal synthesis of zn-mg-based layered double hydroxide coatings for the corrosion protection of copper in chloride and hydroxide media, *Int. J. Miner. Metall. Mater.* 28 (2021) 1991–2000.